CrossMark

J. Fluid Mech. (2018), *vol.* 846, *pp.* 944–965. © Cambridge University Press 2018
doi:10.1017/jfm.2018.304

The influence of two-dimensional temperature modulation on nonlinear Marangoni waves in two-layer films

Alexander A. Nepomnyashchy[1] **and Ilya B. Simanovskii**[1,†]

[1]Department of Mathematics, Technion – Israel Institute of Technology, 32000 Haifa, Israel

(Received 3 September 2017; revised 10 February 2018; accepted 6 April 2018;
first published online 11 May 2018)

The nonlinear dynamics of waves generated by the deformational oscillatory Marangoni instability in a two-layer film under the action of a two-dimensional temperature modulation on the solid substrate is considered. A system of long-wave equations governing the deformations of the upper surface and the interface between the liquids is presented. The long-wave approach is applied. The nonlinear simulations reveal the existence of different dynamic regimes, including stationary, time-periodic and quasi-periodic flows. The general diagrams of the flow regimes are constructed.

Key words: instability, interfacial flows (free surface), thin films

1. Introduction

During the past few decades, a great deal of attention has been paid to the investigation of nonlinear patterns created by instabilities (Cross & Hohenberg 1993). The nonlinear dynamics of systems subjected to oscillatory instabilities is especially rich (Aranson & Kramer 2002).

Applications need the development of instabilities to be controlled. An efficient method of the pattern controlling, first applied in experiments by Chen & Whitehead (1968), is a spatial modulation of the control parameter.

It is necessary to distinguish between patterns created by a short-wave instability, characterized by a non-zero critical wavenumber $k_c \neq 0$, and patterns generated by long-wave instabilities, where the critical wavenumber $k_c = 0$, so that the wavenumber interval of instability is $0 < k < k_m$. The influence of the spatial modulation of the control parameter on stationary short-wave patterns with the moduli of wavevectors close to k_c is rather well understood (see Freund, Pesch & Zimmermann (2011) and references therein). The action of the spatial modulation on oscillatory instabilities was studied on the background of the complex Ginzburg–Landau equation (see Nepomnyashchy & Abarzhi (2010) and references therein). However, long-wave oscillatory instabilities of liquid systems with deformable interfaces cannot be described by the Ginzburg–Landau equation (Nepomnyashchy & Shklyaev 2016).

In the case of a long-wave instability, where disturbances with significantly different wavenumbers are relevant, the prediction of the pattern dynamics is much more

† Email address for correspondence: cesima@technion.ac.il

https://doi.org/10.1017/jfm.2018.304 Published online by Cambridge University Press

difficult. In the absence of a control, the pattern evolution is governed by the nonlinear interaction of disturbances with different wavevectors, which can lead to complex spatio-temporal dynamics. It is tempting to impose a spatial modulation of the control parameter with a prescribed wavelength, which can simplify the dynamics and make it more predictable.

A significant influence of inhomogeneous heating on the development of instabilities has been revealed for flowing films (see Tiwari, Mester & Davis (2007) and Liu & Kabov (2013) and references therein).

The investigation of the impact of spatial modulation on the nonlinear dynamics of Marangoni waves generated by a deformational oscillatory instability in a two-layer liquid film was started in the paper by Nepomnyashchy & Simanovskii (2016). It is known that such a system is subject to an oscillatory instability by heating from below or above, depending on the Biot number (Nepomnyashchy & Simanovskii 2012). A system of long-wave equations governing the deformation of the upper surface and the interface between the liquids in the presence of a temperature modulation of the solid substrate was derived. The nonlinear simulations carried out in the case of one-dimensional temperature modulation revealed the existence of numerous dynamic regimes, including two-dimensional stationary flows and standing waves, three-dimensional standing waves with different spatial periods, and three-dimensional travelling waves.

In the present paper, we consider the nonlinear flow patterns that are developed under the action of two-dimensional temperature modulation. The formulation of the problem is given in § 2. Then § 3 contains a brief description of the Marangoni wave dynamics in the absence of modulation. The results of nonlinear simulations are presented in § 4 (the case of moderate Marangoni number) and § 5 (the case of large Marangoni number). Finally § 6 contains concluding remarks.

2. Formulation of the problem

Consider a system of two superposed layers of immiscible liquids with different physical properties (see figure 1). The bottom layer rests on a solid substrate; the top layer is in contact with the adjacent gas phase. The temperature of the solid substrate is $T_s(x, y)$, and the temperature of the gas is T_g. Herein all variables referring to the bottom layer are marked by subscript 1, and all variables referring to the top layer are marked by subscript 2. The coordinates of the interfaces in a quiescent state are $z = H_m^0$, with $m = 1, 2$. The deformable interfaces are described by the equations $z = H_1(x, y, t)$ (liquid–liquid interface) and $z = H_2(x, y, t)$ (liquid–gas interface). The mth fluid has density ρ_m, kinematic viscosity ν_m, dynamic viscosity $\eta_m = \rho_m \nu_m$, thermal diffusivity χ_m and heat conductivity κ_m. The surface tension coefficients on the lower and upper interfaces, σ_1 and σ_2, are linear functions of temperature T, i.e. $\sigma_1 = \sigma_1^0 - \alpha_1 T$ and $\sigma_2 = \sigma_2^0 - \alpha_2 T$. The problem is considered in the framework of the Boussinesq approximation, i.e. the variation of parameters is neglected (Gershuni & Zhukhovitsky 1976).

Recall that there are two kinds of Marangoni instabilities in liquid layers: a short-wave instability, with critical wavenumber $k_c \neq 0$, and a long-wave deformational instability, with critical wavenumber $k_c = 0$ (see Smith 1966; Takashima 1981; Golovin, Nepomnyashchy & Pismen 1994). For the latter kind of instability, the instability threshold is proportional to the Galileo number $Ga = gH_1^0/(\nu_1 \chi_1)$ (Nepomnyashchy, Simanovskii & Legros 2012), where H_1^0 is the equilibrium thickness of the lower layer; hence it prevails under microgravity conditions and for thin layers. Below, we disregard the effect of gravity, which is negligible for sufficiently thin layers. In the

https://doi.org/10.1017/jfm.2018.304 Published online by Cambridge University Press

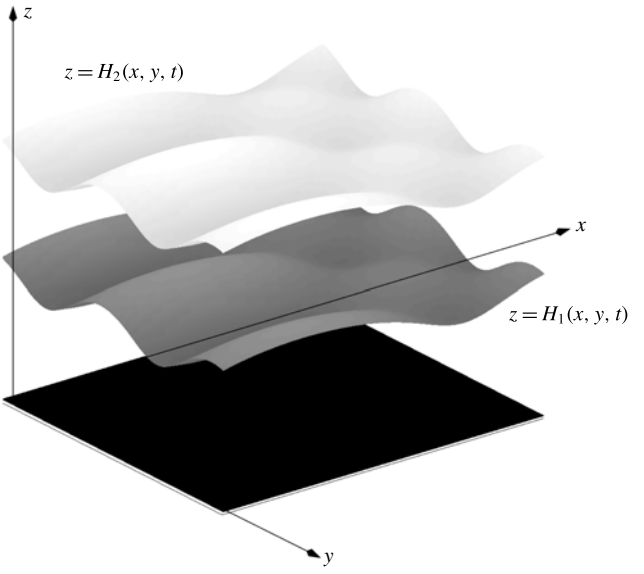


FIGURE 1. Geometric configuration of the region and coordinate axes.

absence of gravity, the long-wave instability has a zero threshold; hence it is always more dangerous than the short-wave one.

We assume that the characteristic spatial scale of the substrate temperature inhomogeneity is large with respect to the layers' thicknesses. The temperature inhomogeneity generates a thermocapillary flow and surface deformations which have the same characteristic spatial scale. That circumstance allows one to apply the long-wave approach, formerly used for studying nonlinear waves created by a long-wave Marangoni instability (Danov *et al.* 1998*a*,*b*,*c*; Pototsky *et al.* 2005; Nepomnyashchy & Simanovskii 2007, 2012).

The natural vertical length scale is H_1^0. The choice of the horizontal length scale, L^*, is arbitrary (see Nepomnyashchy & Simanovskii 2012). We choose

$$\tau^* = \frac{\eta_1 (L^*)^4}{\sigma_1^0 (H_1^0)^3} \tag{2.1}$$

as a time scale and

$$p^* = \frac{\sigma_1^0 H_1^0}{(L^*)^2} \tag{2.2}$$

as a pressure scale.

The non-dimensional parameters of the problem are the Biot number,

$$Bi = \frac{q H_1^0}{\kappa_2}, \tag{2.3}$$

$\eta = \eta_1/\eta_2$, $\kappa = \kappa_1/\kappa_2$, $\sigma = \sigma_2^0/\sigma_1^0$ and $\alpha = \alpha_2/\alpha_1$. Also, we define the local modified Marangoni number,

$$M(x, y) = \frac{\alpha_1 (T_s(x, y) - T_g)}{\sigma_1^0} \left(\frac{L^*}{H_1^0} \right)^2. \tag{2.4}$$

https://doi.org/10.1017/jfm.2018.304 Published online by Cambridge University Press

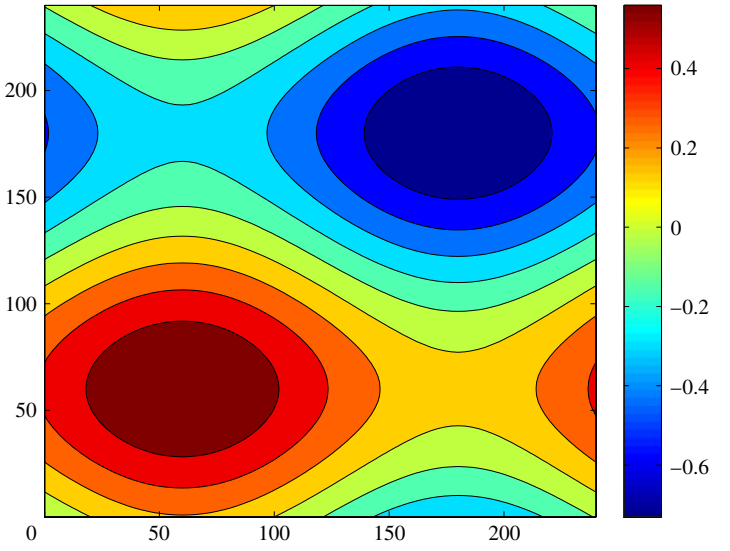


FIGURE 2. (Colour online) Isolines of $h_1(X, Y) - 1$, for $M = -2$, $\delta_X = 0.15$ and $\delta_Y = 0.25$.

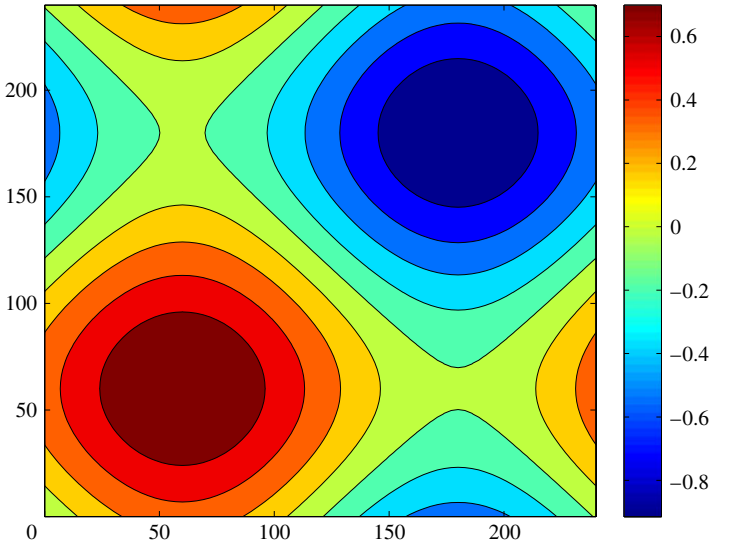


FIGURE 3. (Colour online) Isolines of $h_1(X, Y) - 1$, for $M = -2$ and $\delta_X = \delta_Y = 0.25$.

In the framework of the long-wave approach based on the appropriate rescaling of variables, one can derive a closed system of strongly nonlinear equations for non-dimensional interfacial deformations $h_j = H_j/H_1^0$, with $j = 1, 2$ (Nepomnyashchy & Simanovskii 2016),

$$h_{1\tau} + \nabla_\perp \cdot \boldsymbol{q}_1 = 0, \quad h_{2\tau} + \nabla_\perp \cdot \boldsymbol{q}_2 = 0. \tag{2.5a,b}$$

Here τ is the rescaled non-dimensional time variable, and $\nabla_\perp$ denotes the differentiation with respect to the rescaled non-dimensional horizontal coordinate $\boldsymbol{X} = (X, Y)$.

https://doi.org/10.1017/jfm.2018.304 Published online by Cambridge University Press

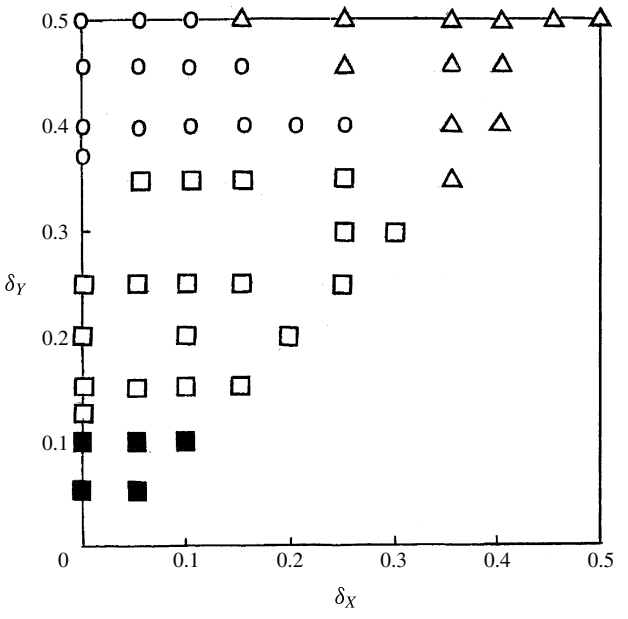


FIGURE 4. General diagram of regimes on the plane (δ_X, δ_Y) for $M = -2$: open squares, stationary pattern; black squares, oscillatory flow at small temperature modulation; open circles, oscillatory flow at large temperature modulation; open triangles, rupture.

Each flux $\boldsymbol{q}_j$, with $j = 1, 2$, is a sum of two terms,

$$\boldsymbol{q}_j = \boldsymbol{q}_j^{\sigma} + \boldsymbol{q}_j^{T}, \quad j = 1, 2. \tag{2.6}$$

The first term, $\boldsymbol{q}_j^{\sigma}$, is the flux generated by the gradients of capillary pressures,

$$\boldsymbol{q}_j^{\sigma} = \sum_{k=1}^{2} f_{jk} \nabla_{\perp} p_k, \quad j = 1, 2 \tag{2.7}$$

(Pototsky *et al.* 2004; Bandyopadhyay, Gulabani & Sharma 2005; Fisher & Golovin 2005), where

$$f_{11} = -\tfrac{1}{3} h_1^3, \quad f_{12} = -\tfrac{1}{2} h_1^2 (h_2 - h_1), \tag{2.8a,b}$$

$$f_{21} = \tfrac{1}{6} h_1^3 - \tfrac{1}{2} h_1^2 h_2, \quad f_{22} = (h_2 - h_1)[h_1^2(\tfrac{1}{2} - \tfrac{1}{3}\eta) + h_1 h_2(-1 + \tfrac{2}{3}\eta) - \tfrac{1}{3}\eta h_2^2], \tag{2.9a,b}$$

$$p_1 = -\nabla_{\perp}^2 h_1 - \sigma \nabla_{\perp}^2 h_2, \tag{2.10}$$

$$p_2 = -\sigma \nabla_{\perp}^2 h_2. \tag{2.11}$$

The second term, $\boldsymbol{q}_j^{T}$, corresponds to the flux generated by the thermocapillary effect,

$$\boldsymbol{q}_1^{T} = -\tfrac{1}{2} h_1^2 \nabla_{\perp}\{M[1 + d(\alpha\kappa - Bi\, h_1)]\}, \tag{2.12}$$

$$\boldsymbol{q}_2^{T} = -\tfrac{1}{2}\eta\alpha\kappa h_2^2 \nabla_{\perp}(Md) + \tfrac{1}{2}(2h_2 - h_1) h_1 \nabla_{\perp}\{M[-1 + Bi\, h_1 d - \alpha\kappa(1 - \eta)d]\}, \tag{2.13}$$

where

$$d(\boldsymbol{X}, \tau) = [\kappa + Bi(1 - \kappa) h_1(\boldsymbol{X}, \tau) + Bi\, \kappa h_2(\boldsymbol{X}, \tau)]^{-1}. \tag{2.14}$$

https://doi.org/10.1017/jfm.2018.304 Published online by Cambridge University Press

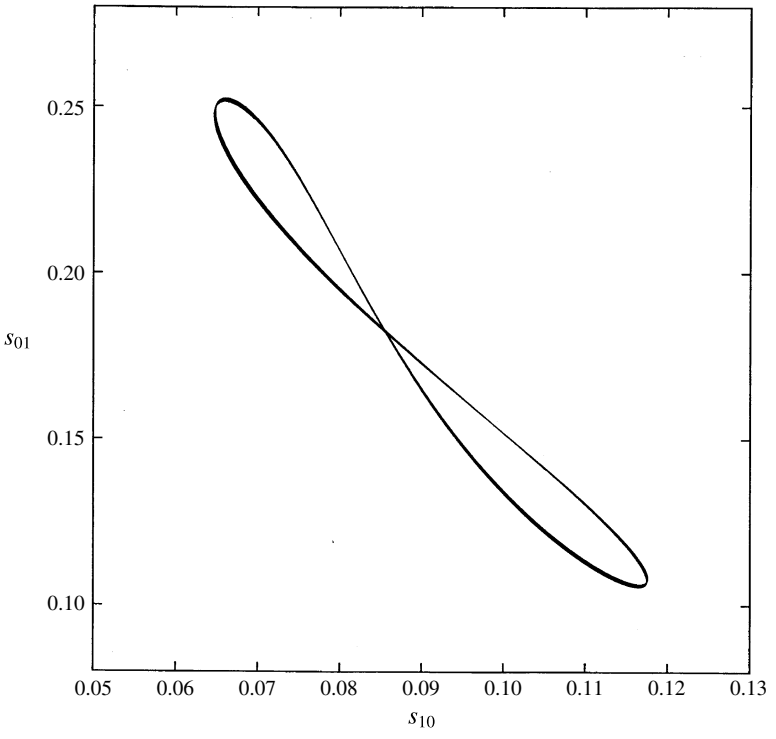


FIGURE 5. Phase trajectory on the plane (s_{10}, s_{01}), for $M = -2$, $\delta_X = 0.05$ and $\delta_Y = 0.1$.

3. Marangoni waves in the absence of modulation

The stability of the mechanical equilibrium and the nonlinear flow regimes in the absence of the substrate temperature modulation ($M(X, Y) = M = \text{const.}$) have been studied by Nepomnyashchy & Simanovskii (2012). It has been shown that, in addition to a monotonic instability leading to the rupture of the film, the two-layer film is subject to an oscillatory instability that generates self-sustained Marangoni waves. The oscillatory instability is developed by heating from below ($M > 0$) if $Bi < Bi_c$, and by heating from above ($M < 0$) if $Bi > Bi_c$, where

$$Bi_c = \frac{1 + \alpha(1 + \eta\kappa a^2 + 2\kappa a)}{a}. \tag{3.1}$$

The oscillatory instability threshold is determined by the formula

$$M_o = M_2 k^2, \tag{3.2}$$

$$M_2 = \frac{2(\kappa + Bi + Bi\,\kappa a)^2}{Bi\,\kappa a(Bi_c - Bi)} \left[\frac{1}{3} + \sigma\left[a(a+1) + \frac{1}{3}(1 + \eta a^3)\right]\right], \tag{3.3}$$

where k is the wavenumber of the disturbance.

If the problem is solved in a finite region $L \times L$ with periodic boundary conditions, then the set of admissible wavevectors is discrete:

$$k_x = mk_0, \quad k_y = nk_0, \quad k_0 = 2\pi/L, \tag{3.4a–c}$$

https://doi.org/10.1017/jfm.2018.304 Published online by Cambridge University Press

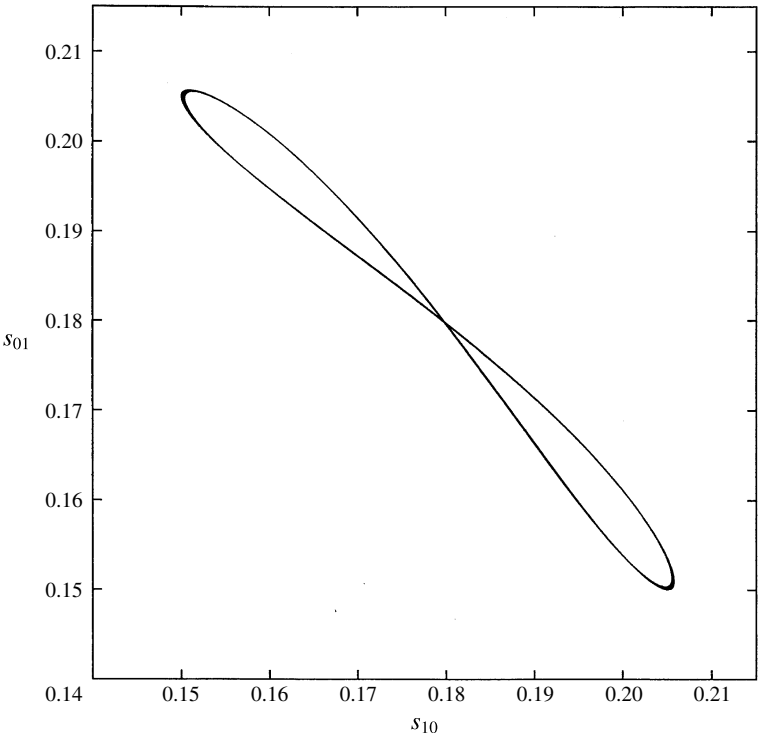


FIGURE 6. Phase trajectory in the plane (s_{10}, s_{01}), for $M = -2$ and $\delta_X = \delta_Y = 0.1$.

where m and n are integers. Therefore,

$$k^2 = (m^2 + n^2)k_0^2. \tag{3.5}$$

Because of the conservation of liquid volumes, the Fourier components of $h_j(X, Y)$ with $m = n = 0$ do not change in time. For an unstable mode, the minimum value of the wavenumber compatible with periodic boundary conditions is k_0. The corresponding modes $(m = \pm 1,\ n = 0)$ and $(m = 0,\ n = \pm 1)$ describe waves with the isolines of $h_j(X, Y)$ parallel to axes X and Y.

Computations have been carried out by Nepomnyashchy & Simanovskii (2012) for the system of Fluorinert FC70 (liquid 1) and silicone oil 10 (liquid 2). The Marangoni convection in that system was studied formerly in microgravity experiments (see e.g. Géoris *et al.* 1999) and by means of a theoretical analysis (Liu *et al.* 2004; Nepomnyashchy *et al.* 2012). It is characterized by the following set of parameters: $\eta = 3.04$, $\kappa = 0.522$, $\alpha = 2$, $\rho = 0.482$, $\sigma = 2.6$. For the system under consideration $\rho < 1$, therefore, there is no Rayleigh–Taylor instability. The computations have been performed for $h = 2.5$, $Bi = 10$ and $L = 240$. Equations (2.5)–(2.13) have been discretized by central differences for spatial derivatives on a grid of 80×80 and solved using an explicit scheme. The Fourier components are

$$c_{mn}(\tau) = \frac{2}{L^2}\int_0^L\int_0^L h_1(X, Y, \tau)\cos\left[\frac{2\pi}{L}(mX + nY)\right] \mathrm{d}X\,\mathrm{d}Y, \tag{3.6}$$

$$s_{mn}(\tau) = \frac{2}{L^2}\int_0^L\int_0^L h_1(X, Y, \tau)\sin\left[\frac{2\pi}{L}(mX + nY)\right] \mathrm{d}X\,\mathrm{d}Y, \tag{3.7}$$

https://doi.org/10.1017/jfm.2018.304 Published online by Cambridge University Press

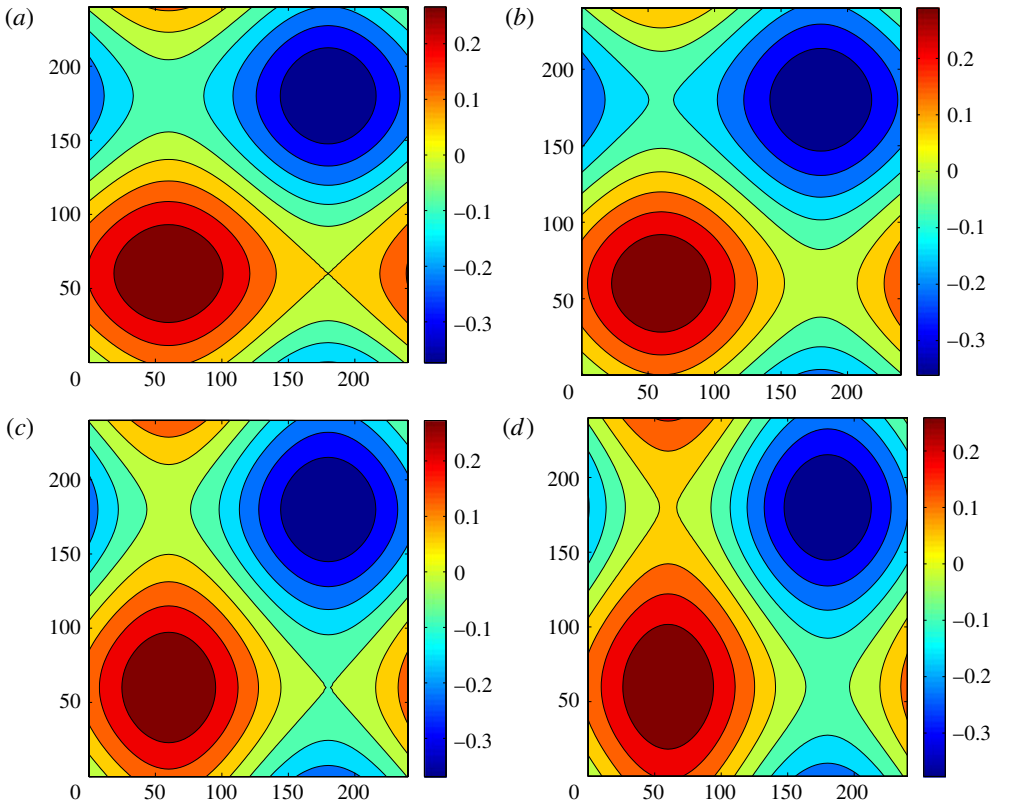


FIGURE 7. (Colour online) Snapshots of the isolines of $h_1(X, Y, \tau) - 1$, for $M = -2$ and $\delta_X = \delta_Y = 0.1$: (*a*) $\tau = 2410\,097$; (*b*) $\tau = 2410\,200$; (*c*) $\tau = 2410\,385$; (*d*) $\tau = 2410\,500$.

where m and n are integers. Also, variables

$$r_{mn}(\tau) = \sqrt{c_{mn}^2(\tau) + s_{mn}^2(\tau)}, \tag{3.8}$$

which characterize the amplitudes of the corresponding complex Fourier harmonics, and quantities

$$h_{max,j}(\tau) = \max_{X,Y} h_j(X, Y, \tau), \quad j = 1, 2, \tag{3.9}$$

which describe the deformations of the surfaces, have been used.

For $Bi = 10$, the mechanical equilibrium state is unstable with respect to oscillatory disturbances by heating from above. In the region $L \times L$ with periodic boundary conditions, the linear stability theory (see (3.2) and (3.3)) predicts the instability threshold $M_* = M_o(k_0) \approx -1.02$. Below the threshold, the system tends to the mechanical equilibrium state. Above the threshold, the nonlinear development of the instability creates a wave pattern known as alternating rolls. That motion is a superposition of two periodic standing waves with wavevectors directed along the axes X and Y. The oscillations of waves with orthogonal wavevectors have a mutual phase shift corresponding to a quarter of a period, $T/4$. The mean values of the

https://doi.org/10.1017/jfm.2018.304 Published online by Cambridge University Press

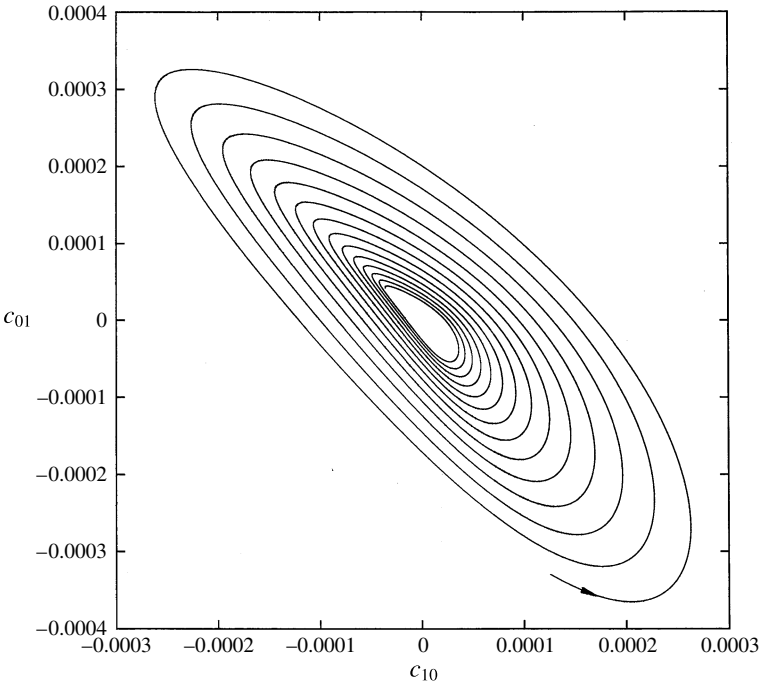


FIGURE 8. Decay of Fourier component $c_{10}(\tau)$, $c_{01}(\tau)$.

Fourier components $s_{10}(\tau)$, $c_{10}(\tau)$, $s_{01}(\tau)$ and $c_{01}(\tau)$ are equal to zero; the amplitudes of both standing waves are equal,

$$\max_{\tau} r_{10}(\tau) = \max_{\tau} r_{01}(\tau). \tag{3.10}$$

The quantities $h_{max,j}(\tau)$, $j = 1, 2$, oscillate with period $T/4$.

4. Nonlinear flow regimes for moderate $|M|$

In this section, we discuss the nonlinear regimes observed in the case of a spatially periodic temperature modulation. The most interesting dynamics is expected when the problem has a definite symmetry, which leads to the enhancement of the dimension of the central manifold near the instability point. In the present paper, we investigate the case $L_x = L_y = L$ when the computational region has a symmetry $X \to Y$ and $Y \to X$. Correspondingly, we apply a special disturbance of the kind

$$M(X) = M\left(1 + \delta_X \sin\frac{2\pi X}{L} + \delta_Y \sin\frac{2\pi Y}{L}\right). \tag{4.1}$$

Note that function (4.1) is symmetric with respect to axes $X = L/4$, $X = 3L/4$, $Y = L/4$ and $Y = 3L/4$.

Let us note that the problem is characterized by a large number of non-dimensional parameters, and the investigation of their influence is beyond the scope of the present paper. The computations are carried out for a typical system of liquids appropriate for experiments, namely, the system of liquids Fluorinert FC70/silicone oil 10, and the

https://doi.org/10.1017/jfm.2018.304 Published online by Cambridge University Press

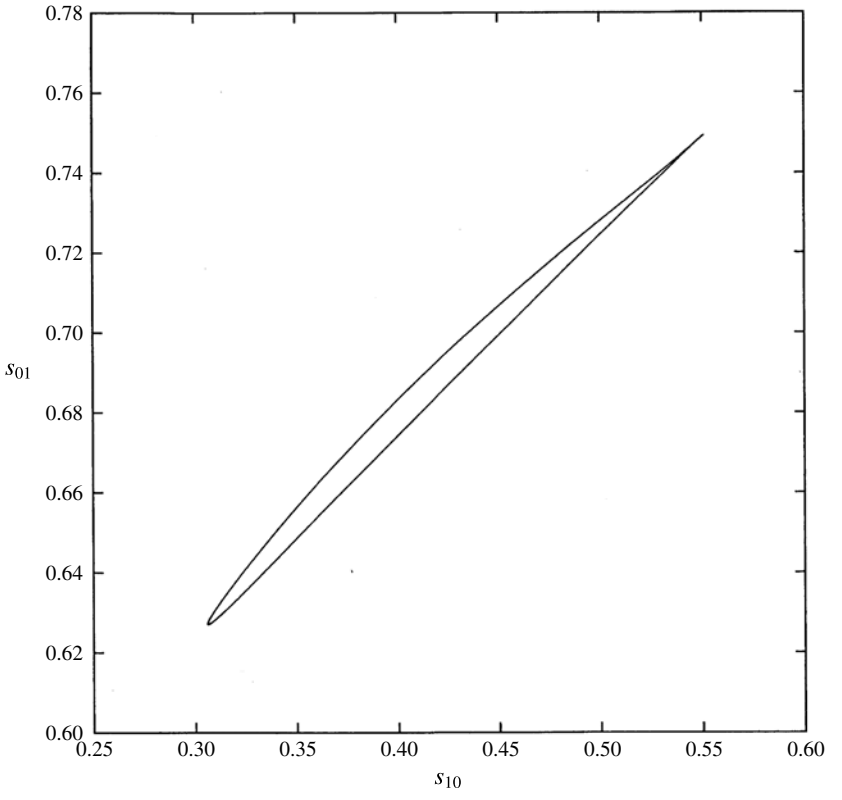


FIGURE 9. Phase trajectory in the plane (s_{10}, s_{01}), for $M = -2$, $\delta_X = 0.25$ and $\delta_Y = 0.4$.

values of parameters ($h = 2.5$, $Bi = 10$, $L = 240$) formerly used by Nepomnyashchy & Simanovskii (2012). The same numerical method is applied.

We are interested in the case of heating from above ($M < 0$), where there is no film rupture in the absence of a temperature modulation. It is sufficient to take $\delta_X > 0$ and $\delta_Y > 0$, because the change of the sign of δ_X or δ_Y is obtained by a translation $X \to X + L/2$ or $Y \to Y + L/2$, correspondingly. Because of the symmetry of the problem with respect to the transformation $X \to Y$ and $Y \to X$, it is sufficient to consider the case $\delta_Y \geqslant \delta_X$.

4.1. *Stationary flow*

As mentioned in § 3, in the absence of modulation, no flow is observed in the subcritical region $|M| < M_*$. The inhomogeneity of the substrate temperature generates a stationary thermocapillary flow, which creates a stationary deformation of the surfaces $h_j = h_j(X, Y)$, $j = 1, 2$. For moderate values of δ_X and δ_Y, the stationary flow generated by temperature modulation is more stable than the mechanical equilibrium in the absence of modulation: it is observed in a certain interval of $|M| > M_*$. The symmetry properties of the fields $h_j(X, Y)$ coincide with those of function $M(X, Y)$, i.e. they are symmetric with respect to the axes $X = L/4$, $X = 3L/4$, $Y = L/4$ and $Y = 3L/4$ (see figure 2). For that pattern, Fourier components c_{10} and c_{01} vanish, while s_{10} and s_{01} are non-zero.

https://doi.org/10.1017/jfm.2018.304 Published online by Cambridge University Press

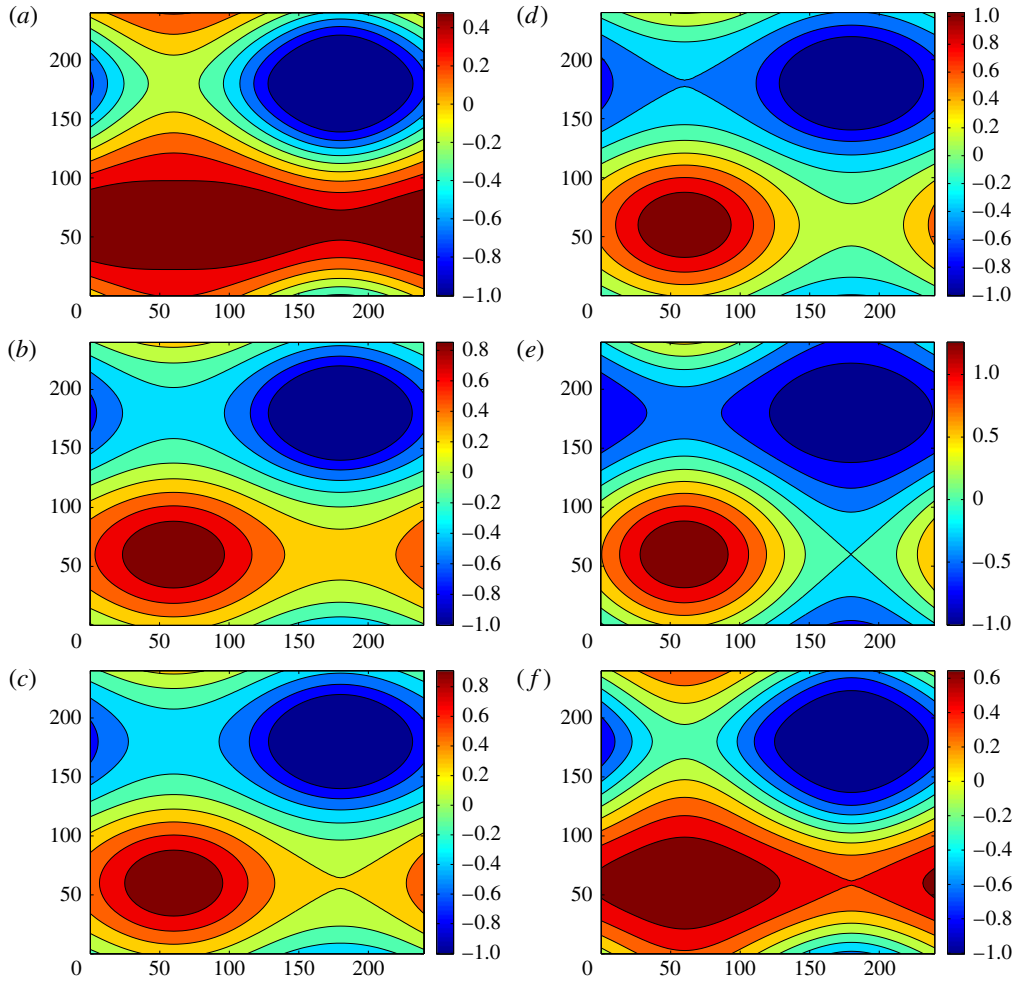


FIGURE 10. (Colour online) Snapshots of the isolines of $h_1(X, Y, \tau) - 1$, for $M = -2$, $\delta_X = 0.25$ and $\delta_Y = 0.4$: (*a*) $\tau = 2010\,099$; (*b*) $\tau = 2010\,185$; (*c*) $\tau = 2010\,195$; (*d*) $\tau = 2010\,220$; (*e*) $\tau = 2010\,366$; (*f*) $\tau = 2010\,507$.

In the case $\delta_X = \delta_Y$, one observes a stationary square pattern, which is symmetric also with respect to axes $X = Y$ and $X = L - Y$ (see figure 3); for that pattern, $s_{10} = s_{01}$.

The stationary flows are observed in a rather large region in the plane (δ_X, δ_Y). In figure 4, that flow regime is shown by open squares.

4.2. *Oscillatory flows for smaller values of* δ_X *and* δ_Y

With a decrease of δ_X and δ_Y, an oscillatory instability of a stationary flow appears, which creates a time-periodic flow regime. The Fourier harmonics $s_{10}(\tau)$ and $s_{01}(\tau)$ oscillate without changing their signs, mostly out of phase. The phase trajectory is asymmetric if $\delta_X \neq \delta_Y$ (figure 5), and symmetric if $\delta_X = \delta_Y$ (figure 6). One observes time-periodic pulsation of the cell (see figure 7). The Fourier components $c_{10}(\tau)$ and $c_{01}(\tau)$ decay in an oscillatory way (figure 8). In the case $\delta_X = 0$ and $\delta_Y \neq 0$, we obtain a time-periodic two-dimensional standing wave.

https://doi.org/10.1017/jfm.2018.304 Published online by Cambridge University Press

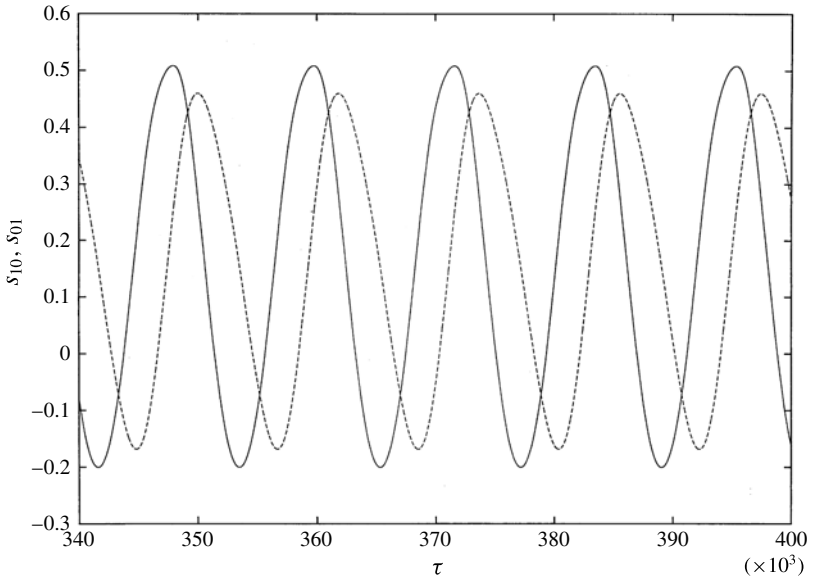


FIGURE 11. Oscillations of $s_{10}(\tau)$, $s_{01}(\tau)$, for $M = -6$ and $\delta_X = \delta_Y = 0.1$.

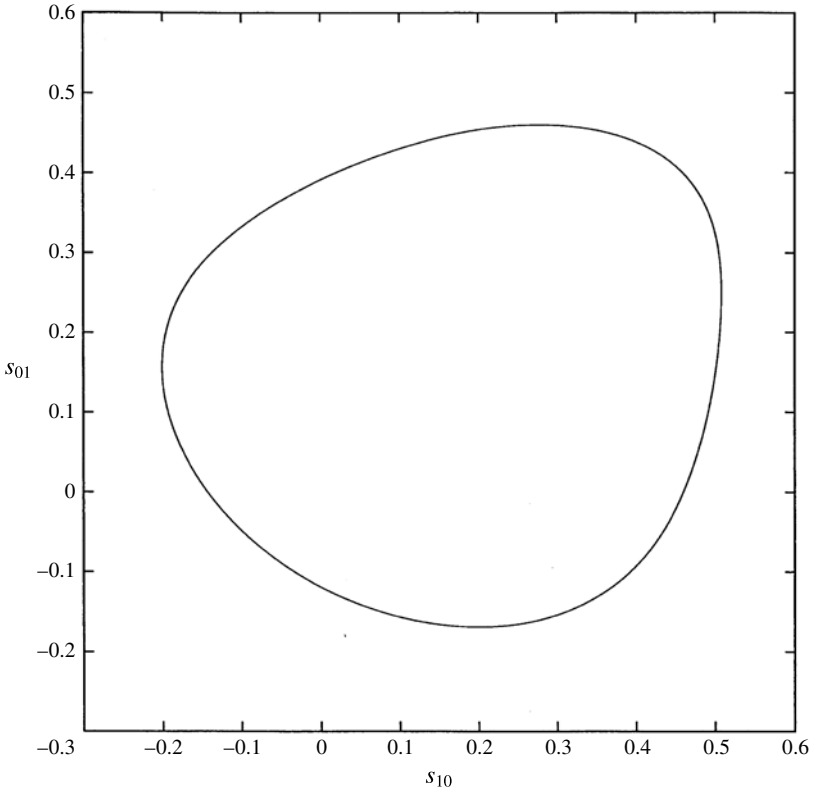


FIGURE 12. Phase trajectory on the plane (s_{10}, s_{01}), for $M = -6$ and $\delta_X = \delta_Y = 0.1$.

https://doi.org/10.1017/jfm.2018.304 Published online by Cambridge University Press

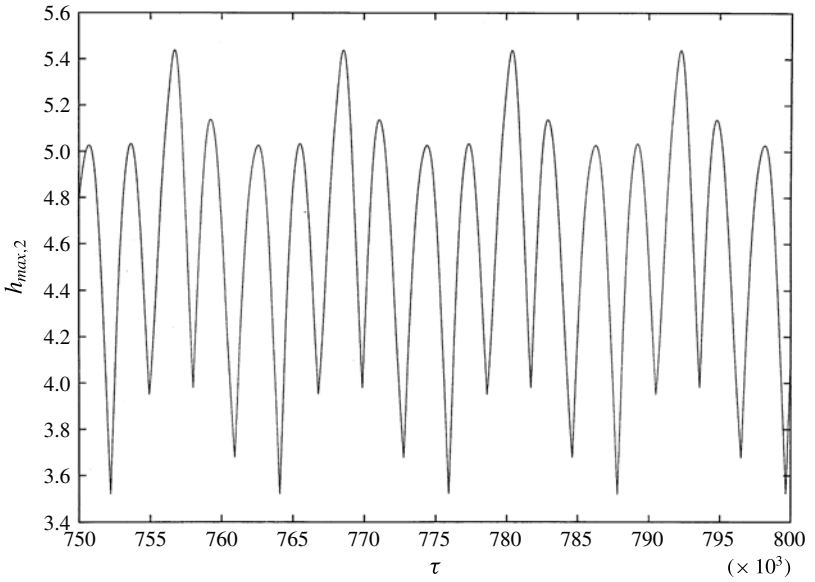


FIGURE 13. Dependence $h_{max,2}(\tau)$, for $M = -6$ and $\delta_X = \delta_Y = 0.1$.

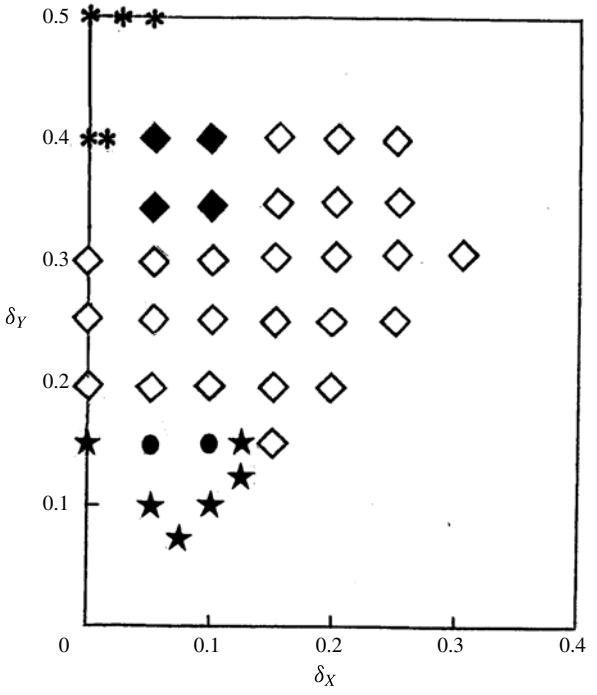


FIGURE 14. General diagram of regimes on the plane (δ_X, δ_Y), for $M = -6$: stars, periodic oscillatory flow; black circles, quasi-periodic oscillatory flow; open diamonds, periodic two-cell flow; black diamonds, quasi-periodic two-cell flow; asterisks, periodic three-cell flow.

https://doi.org/10.1017/jfm.2018.304 Published online by Cambridge University Press

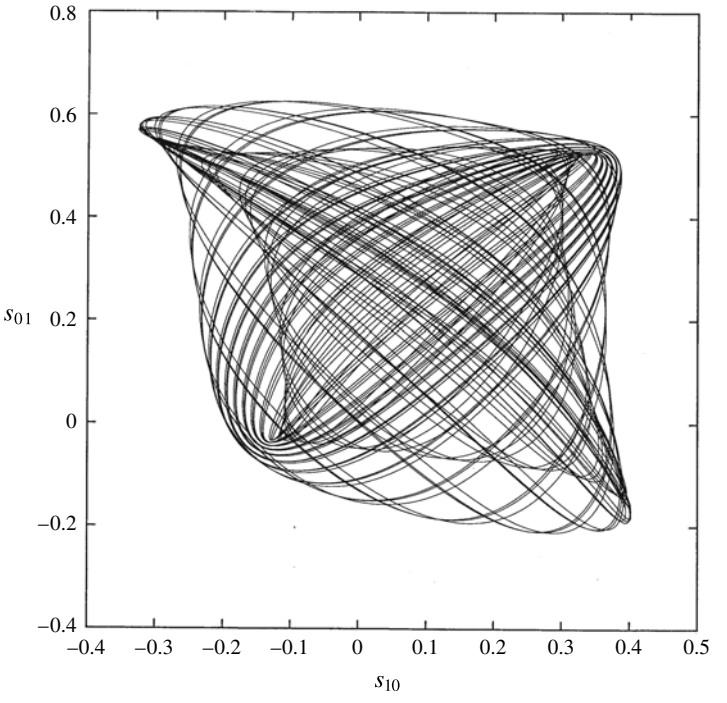


FIGURE 15. Phase trajectory on the plane (s_{10}, s_{01}), for $M = -6$, $\delta_X = 0.05$ and $\delta_Y = 0.15$.

With a further decrease of δ_X and δ_Y, the oscillation amplitudes of the Fourier harmonics s_{10} and s_{01} become larger than their mean values; thus they change their signs, so that the pattern evolution resembles alternating rolls.

The region of the time-periodic oscillatory regime discussed above is shown in figure 4 by black squares.

4.3. *Oscillatory flows for larger values of δ_X and δ_Y*

With the growth of δ_Y, another oscillatory instability of stationary flows takes place. The Fourier harmonics s_{10} and s_{01} oscillate mostly in phase (see figure 9), while $c_{10} = c_{01} = 0$. The characteristic snapshots of height isolines are shown in figure 10. The corresponding region in the plane (δ_X, δ_Y) is shown in figure 4 by open circles. In the limit $\delta_X \to 0$, this type of oscillation tends to a wave travelling in the X-direction.

For even larger values of δ_X and δ_Y, the thickness of the bottom layer becomes equal to zero in the course of the development of instability. Note that a self-consistent consideration of a liquid layer rupture cannot be carried out in the framework of model (2.5)–(2.14): the contributions of intermolecular forces have to be included (Fisher & Golovin 2005; Pototsky *et al.* 2005; Nepomnyashchy & Simanovskii 2006). Therefore, we stopped the simulations when

$$h_{min,1}(\tau) = \min_{X,Y} h_1(X, Y, \tau) \tag{4.2}$$

approached zero ($h_{min,1}(\tau) < 10^{-19}$). The region where the model used predicts film rupture is shown in figure 4 by triangles. In our computations, we never observed the rupture of the upper layer preceding the rupture of the lower layer. Note that in the

https://doi.org/10.1017/jfm.2018.304 Published online by Cambridge University Press

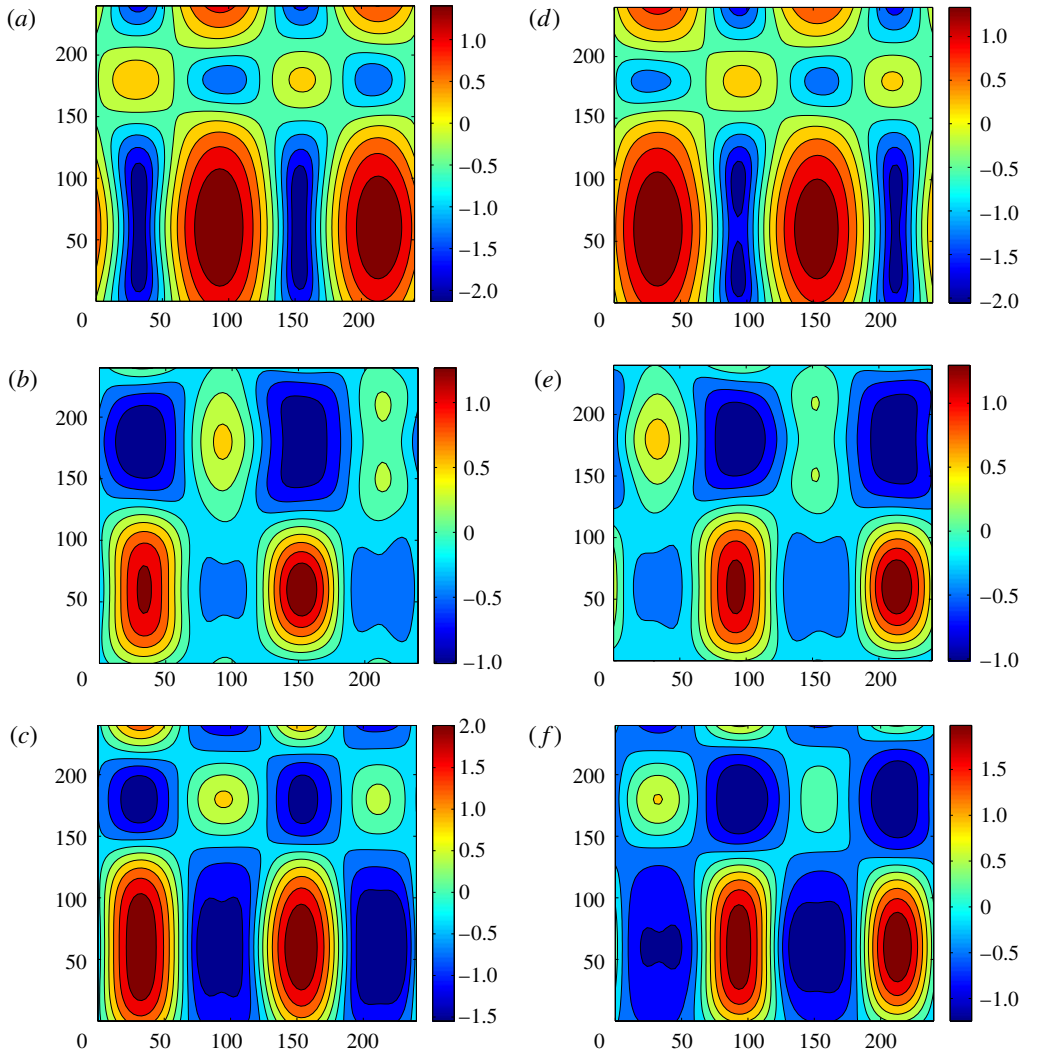


FIGURE 16. (Colour online) Snapshots of the isolines of $h_2(X, Y, \tau) - h$, for $M = -6$, $\delta_X = 0.05$ and $\delta_Y = 0.25$: (*a*) $\tau = 2100\,000$; (*b*) $\tau = 2100\,117$; (*c*) $\tau = 2100\,185$; (*d*) $\tau = 2100\,255$; (*e*) $\tau = 2100\,364$; (*f*) $\tau = 2100\,399$.

case of interfacial heating, both kinds of ruptures were observed (Nepomnyashchy & Simanovskii 2017).

5. Nonlinear flow regimes for large $|M|$

Far from the instability threshold, the sequence of nonlinear flow regimes is quite different. At $M = -6$, we did not find a region where the flow is stationary. At sufficiently small δ_X and δ_Y, we obtain a time-periodic oscillatory flow with a phase shift between oscillations of $s_{10}(\tau)$ and $s_{01}(\tau)$ close to a quarter of a period, $T/4$ (see figure 11), which is quite similar to alternating rolls observed as $\delta_X = \delta_Y = 0$. However, now the phase trajectory in the plane (s_{10}, s_{01}) is not symmetric even in the case $\delta_X = \delta_Y$ (see figure 12). While for 'usual' alternating rolls the oscillation

https://doi.org/10.1017/jfm.2018.304 Published online by Cambridge University Press

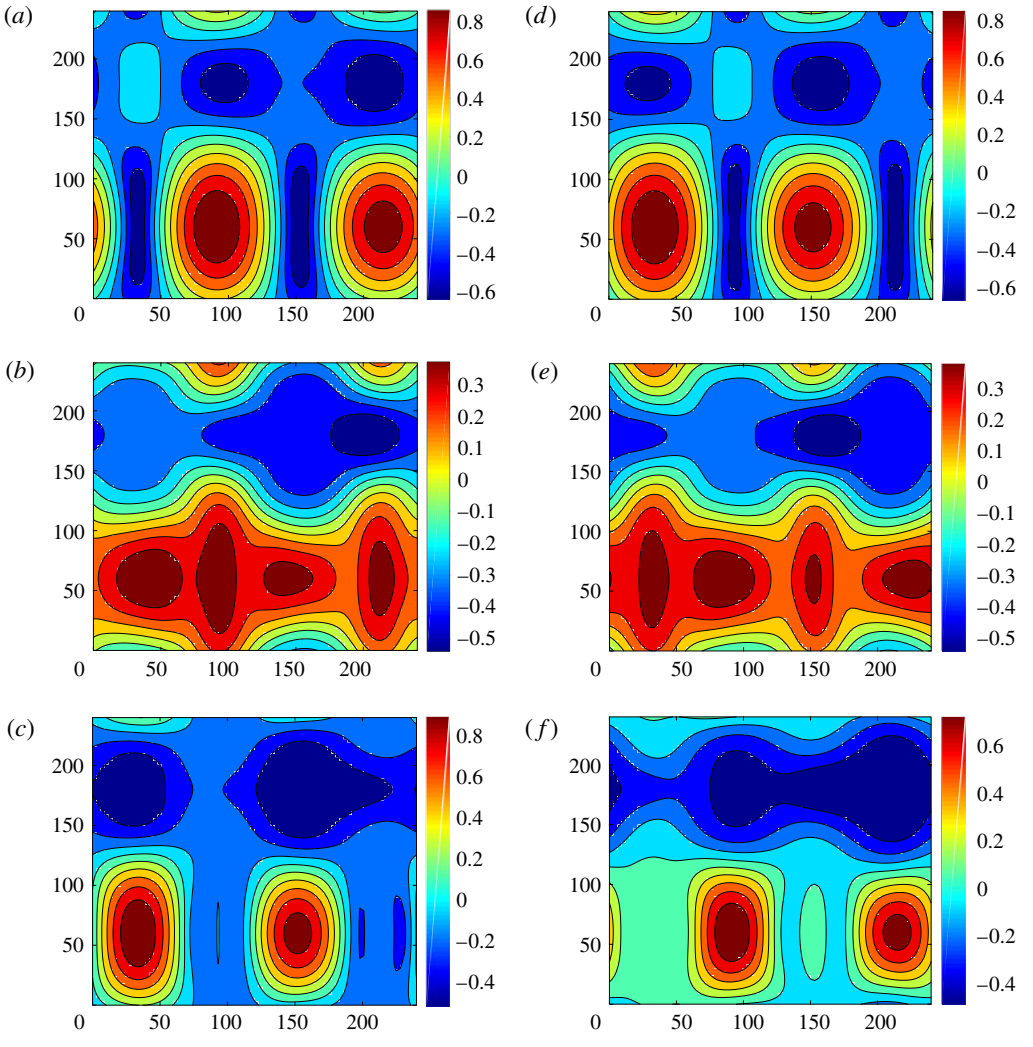


FIGURE 17. (Colour online) Snapshots of the isolines of $h_1(X, Y, \tau) - 1$, for $M = -6$, $\delta_X = 0.05$ and $\delta_Y = 0.25$: (*a*) $\tau = 2100\,000$; (*b*) $\tau = 2100\,117$; (*c*) $\tau = 2100\,185$; (*d*) $\tau = 2100\,255$; (*e*) $\tau = 2100\,364$; (*f*) $\tau = 2100\,399$.

period of quantities $h_{max,j}(\tau)$ is equal to $T/4$, that period is now T: the maxima of $h_{max,j}(\tau)$ corresponding to maxima of $|s_{10}|(\tau)$ and $|s_{01}|(\tau)$ are not equal to each other (see figure 13). Note that $c_{10}(\tau)$ and $c_{01}(\tau)$ decay; therefore, the structure keeps the symmetry with respect to two vertical axes and two horizontal axes, corresponding to the symmetry of the temperature modulation (4.1). The flow regime described above is shown in figure 14 by stars.

In a certain region of parameters δ_X and δ_Y, indicated by black circles in figure 14, quasi-periodic oscillations are observed (see figure 15). The Fourier component $s_{10}(\tau)$ oscillates with the mean frequency ω_{10} slightly larger than the mean frequency ω_{01} of $s_{01}(\tau)$. Their nonlinear interaction creates modulation of oscillations with the characteristic time scale $2\pi/(\omega_{10} - \omega_{01})$, which is much larger than $2\pi/\omega_{10}$ and $2\pi/\omega_{01}$.

https://doi.org/10.1017/jfm.2018.304 Published online by Cambridge University Press

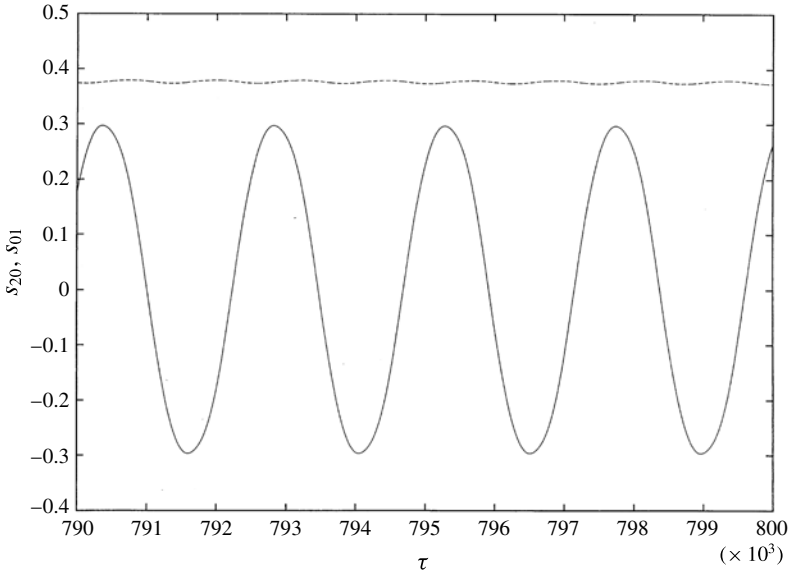


FIGURE 18. Oscillations of $s_{20}(\tau)$ (solid line) and $s_{01}(\tau)$ (dashed line), for $M = -6$, $\delta_X = 0.05$ and $\delta_Y = 0.25$.

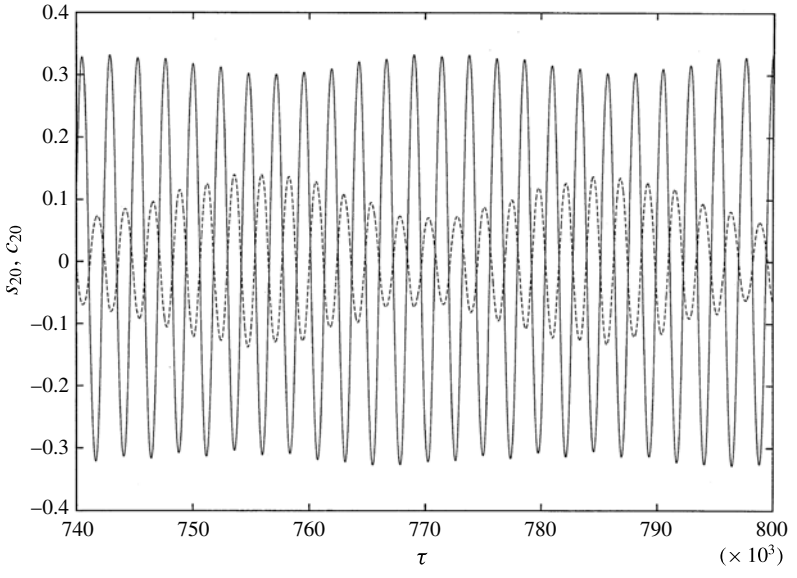


FIGURE 19. Oscillations of $s_{20}(\tau)$ (solid line) and $c_{20}(\tau)$ (dashed line), for $M = -6$, $\delta_X = 0.05$ and $\delta_Y = 0.35$.

For larger values of δ_Y, a 'two-cell' time-periodic regime with $|s_{20}| > |s_{10}|$ is developed (see figures 16 and 17). The symmetry with respect to horizontal axes is retained, but the symmetry with respect to vertical axes is broken. The oscillations of $c_{20}(\tau)$ and $s_{20}(\tau)$ are proportional, that is, a standing wave. Owing to the nonlinearity of the equations, oscillations of $c_{20}(\tau)$ and $s_{20}(\tau)$ generate oscillations of s_{01} with a doubled frequency (see figure 18). That regime is indicated in figure 14 by open diamonds.

https://doi.org/10.1017/jfm.2018.304 Published online by Cambridge University Press

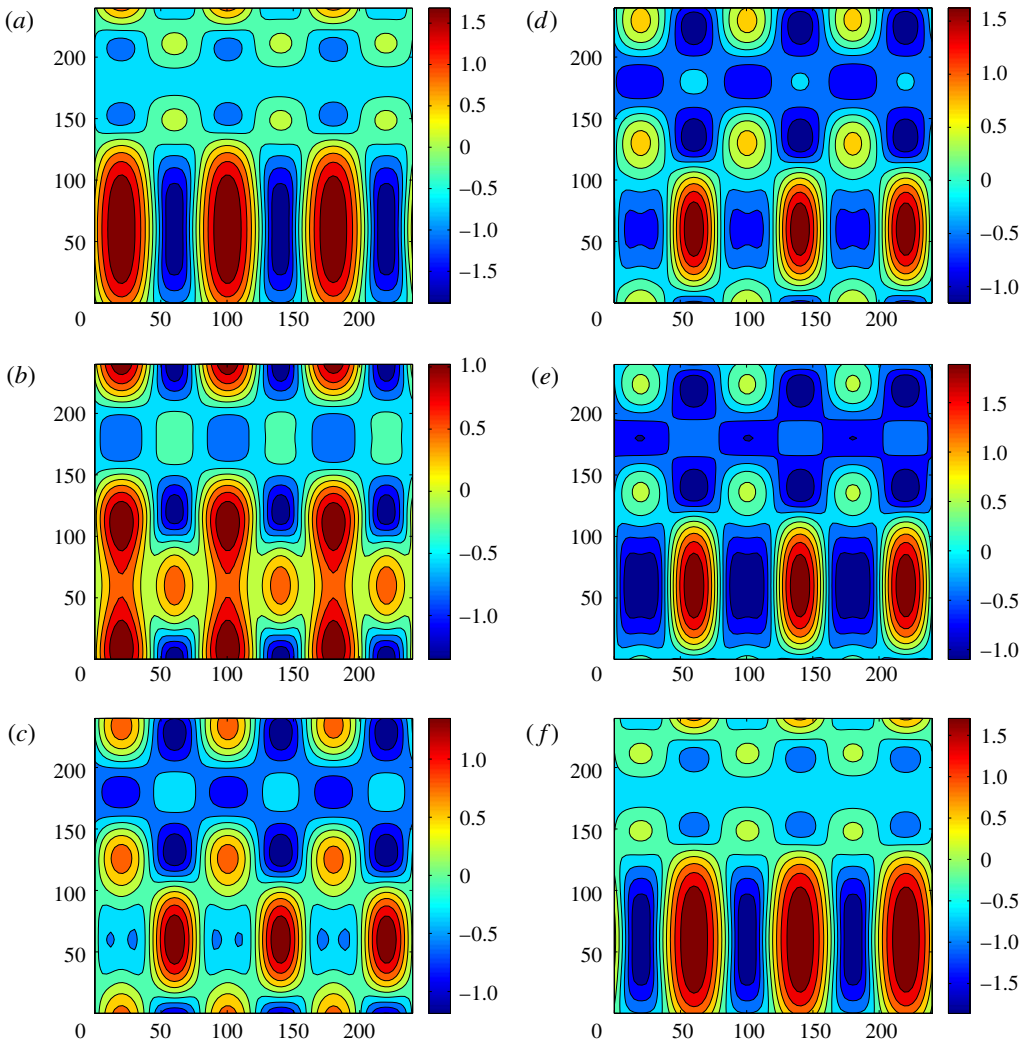


FIGURE 20. (Colour online) Snapshots of the isolines of $h_2(X, Y, \tau) - h$, $M = -6$, $\delta_X = 0.01$ and $\delta_Y = 0.4$: (*a*) $\tau = 2020\,940$; (*b*) $\tau = 2020\,960$; (*c*) $\tau = 2020\,968$; (*d*) $\tau = 2020\,971$; (*e*) $\tau = 2020\,976$; (*f*) $\tau = 2020\,989$.

With a further growth of δ_Y, the standing waves become quasi-periodic (see figure 19). The region of that regime is shown in figure 14 by black diamonds.

Even more short-scale time-periodic standing waves are observed for larger values of δ_Y (see figures 20–22). That 'three-cell' regime is quite similar to the periodic regime described above, but now the proportional Fourier components $s_{30}(\tau)$ and $c_{30}(\tau)$ prevail. Its existence region is indicated by asterisks in figure 14.

6. Conclusions

The impact of a two-dimensional temperature modulation on the nonlinear Marangoni waves in a two-layer liquid system has been studied in the framework of

https://doi.org/10.1017/jfm.2018.304 Published online by Cambridge University Press

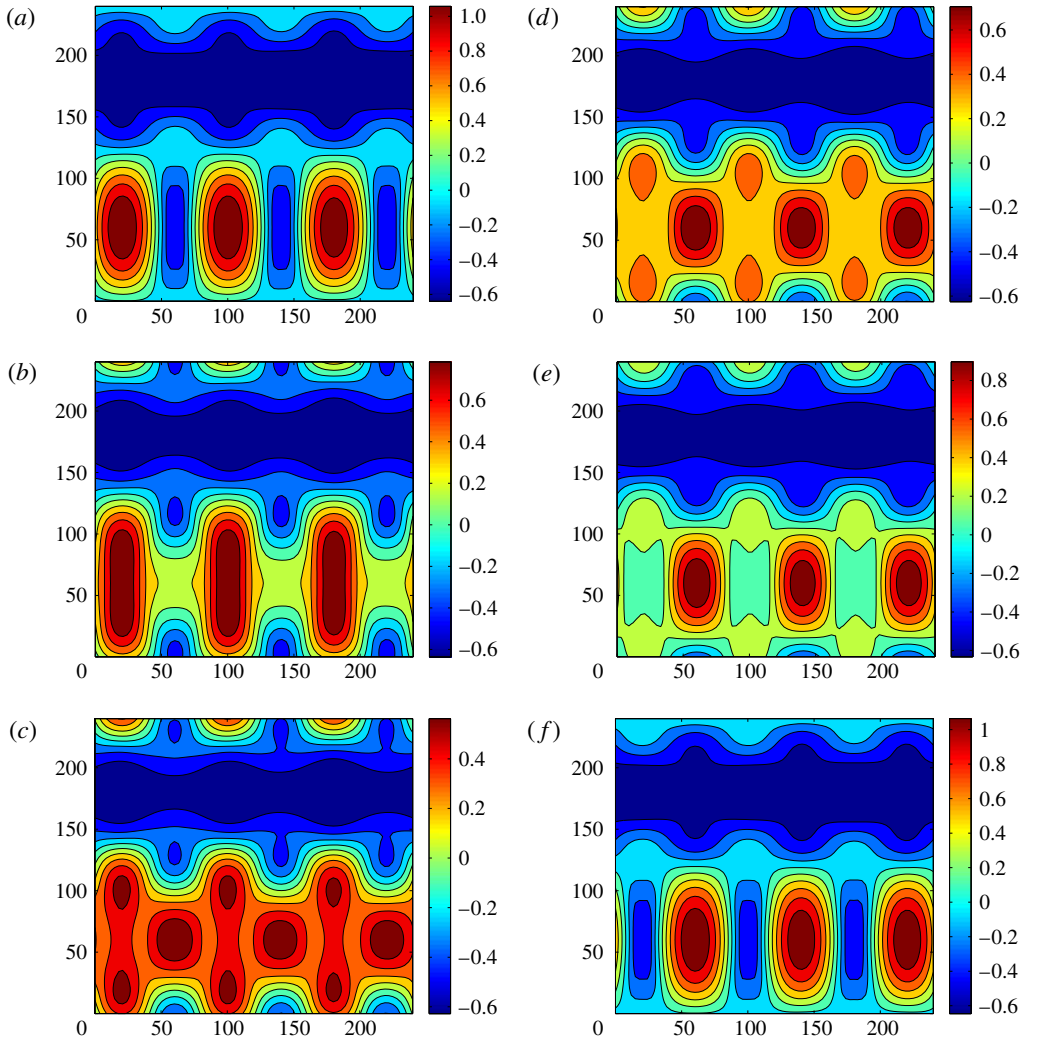


FIGURE 21. (Colour online) Snapshots of the isolines of $h_1(X, Y, \tau) - 1$, for $M = -6$, $\delta_X = 0.01$ and $\delta_Y = 0.4$: (*a*) $\tau = 2020\,940$; (*b*) $\tau = 2020\,960$; (*c*) $\tau = 2020\,968$; (*d*) $\tau = 2020\,971$; (*e*) $\tau = 2020\,976$; (*f*) $\tau = 2020\,989$.

a long-wave approach. The problem is reduced to a system of two coupled nonlinear equations for the surface deformations.

The computations have been carried out for the system of Fluorinert FC70 (liquid 1) and silicone oil 10 (liquid 2). According to Géoris *et al.* (1999), $\sigma_1^0 = 6.9 \times 10^{-3}$ N m^{-1} and $\alpha_1 = 2.7 \times 10^{-5}$ N m^{-1} K^{-1}. Applying the definition of the Marangoni number (2.4), we find that the value $M = -6$ used in our computations corresponds to the temperature difference $T_g - T_s = 1$ K if $L^*/H_1^0 = 9.6$, hence the aspect ratio of the region $LL^*/H_1^0 \approx 230$.

A number of nonlinear regimes have been revealed and investigated. Among them are stationary patterns, different types of time-periodic oscillations, as well as flows quasi-periodic in time. It is found that two-dimensional modulations can lead to the appearance of new regimes in comparison with the one-dimensional case. It is

https://doi.org/10.1017/jfm.2018.304 Published online by Cambridge University Press

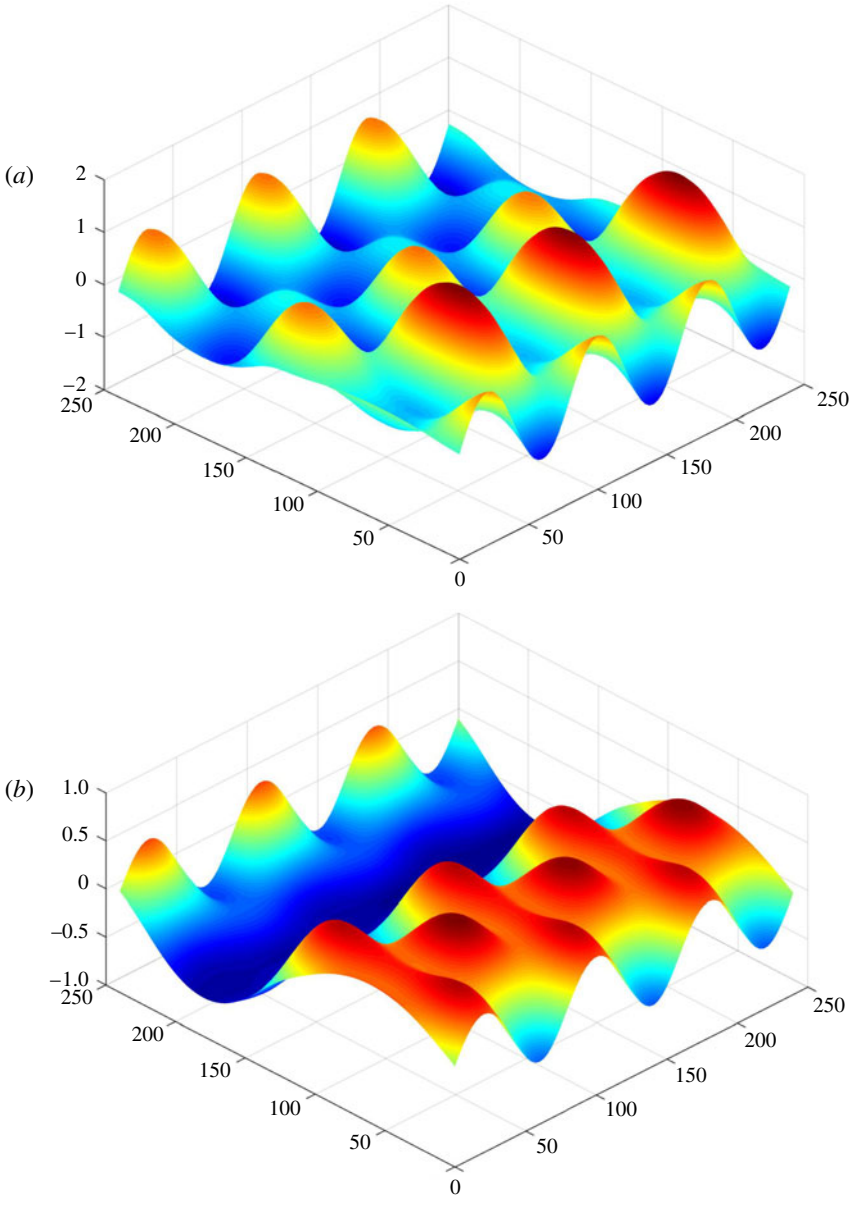


FIGURE 22. (Colour online) Shapes of (*a*) the upper surface $z = h_2(X, Y, \tau)$ and (*b*) the interface $z = h_1(X, Y, \tau)$, for $M = -6$, $\delta_X = 0.01$ and $\delta_Y = 0.4$.

shown that the sequence of nonlinear flow regimes for sufficiently large values of the Marangoni number is quite different in comparison with the regimes obtained for moderate values of the Marangoni number. Specifically, it is shown that for sufficiently large values of the Marangoni number, an increase of δ_Y can lead to the development of periodic and quasi-periodic multi-cell flows. Under certain conditions, a rupture of one of the layers is observed. The general diagrams of the flow regimes are presented.

https://doi.org/10.1017/jfm.2018.304 Published online by Cambridge University Press

REFERENCES

ARANSON, I. S. & KRAMER, L. 2002 The world of the complex Ginzburg–Landau equation. *Rev. Mod. Phys.* **74**, 99–143.

BANDYOPADHYAY, D., GULABANI, R. & SHARMA, A. 2005 Instability and dynamics of thin liquid bilayers. *Ind. Engng Chem. Res.* **44**, 1259–1272.

CHEN, M. M. & WHITEHEAD, J. A. 1968 Evolution of two-dimensional periodic Rayleigh convection cells of arbitrary wave-numbers. *J. Fluid Mech.* **31**, 1–15.

CROSS, M. C. & HOHENBERG, P. C. 1993 Pattern formation outside of equilibrium. *Rev. Mod. Phys.* **65**, 851–1112.

DANOV, K. D., ALLEBORN, N., RASZILLIER, H. & DURST, F. 1998*a* The stability of evaporating thin liquid films in the presence of surfactant. I. Lubrication approximation and linear analysis. *Phys. Fluids* **10**, 131–143.

DANOV, K. D., PAUNOV, V. N., ALLEBORN, N., RASZILLIER, H. & DURST, F 1998*b* Stability of evaporating two-layered liquid film in the presence of surfactant. I. The equations of lubrication approximation. *Chem. Engng Sci.* **53**, 2809–2822.

DANOV, K. D., PAUNOV, V. N., STOYANOV, S. D., ALLEBORN, N., RASZILLIER, H. & DURST, F. 1998*c* Stability of evaporating two-layered liquid film in the presence of surfactant: II. Linear analysis. *Chem. Engng Sci.* **53**, 2823–2837.

FISHER, L. S. & GOLOVIN, A. A. 2005 Nonlinear stability analysis of a two-layer thin liquid film: dewetting and autophobic behavior. *J. Colloid Interface Sci.* **291**, 515–528.

FREUND, G., PESCH, W. & ZIMMERMANN, W. 2011 Rayleigh–Bénard convection in the presence of spatial temperature modulation. *J. Fluid Mech.* **673**, 318–348.

GÉORIS, PH., HENNENBERG, M., LEBON, G. & LEGROS, J. C. 1999 Investigation of thermocapillary convection in a three-liquid-layer systems. *J. Fluid Mech.* **389**, 209–228.

GERSHUNI, G. Z. & ZHUKHOVITSKY, E. M. 1976 *Convective Stability of Incompressible Fluid*. Keter.

GOLOVIN, A. A., NEPOMNYASHCHY, A. A. & PISMEN, L. M. 1994 Interaction between short-scale Marangoni convection and long-scale deformational instability. *Phys. Fluids* **6**, 34–48.

LIU, Q. S., ZHOU, B. H., NGUYEN THI, H. & HU, W. R. 2004 Instability of two-layer Rayleigh Bénard convection with interfacial thermocapillary effect. *Chin. Phys. Lett.* **21**, 686–688.

LIU, R. & KABOV, O. A. 2013 Effect of mutual location and the shape of heaters on the stability of thin films flowing over locally heated surfaces. *Intl J. Heat Mass Transfer* **65**, 23–32.

NEPOMNYASHCHY, A. A. & ABARZHI, S. I. 2010 Monochromatic waves induced by large-scale parametric forcing. *Phys. Rev.* E **81**, 037202.

NEPOMNYASHCHY, A. A. & SHKLYAEV, S. 2016 Longwave oscillatory patterns in liquids: outside the world of the complex Ginzburg–Landau equation. *J. Phys. A: Math. Gen.* **49**, 053001.

NEPOMNYASHCHY, A. A. & SIMANOVSKII, I. B. 2006 Decomposition of a two-layer thin liquid film flowing under the action of Marangoni stresses. *Phys. Fluids* **18**, 112101.

NEPOMNYASHCHY, A. A. & SIMANOVSKII, I. B. 2007 Marangoni instability in ultrathin two-layer films. *Phys. Fluids* **19**, 112103.

NEPOMNYASHCHY, A. A. & SIMANOVSKII, I. B. 2012 Nonlinear Marangoni waves in a two-layer film in the presence of gravity. *Phys. Fluids* **24**, 032101.

NEPOMNYASHCHY, A. A. & SIMANOVSKII, I. B. 2016 Marangoni waves in two-layer films under the action of spatial temperature modulation. *J. Fluid Mech.* **805**, 322–354.

NEPOMNYASHCHY, A. A. & SIMANOVSKII, I. B. 2017 Novel criteria for the development of monotonic and oscillatory instabilities in a two-layer film. *Phys. Fluids* **29**, 092104.

NEPOMNYASHCHY, A., SIMANOVSKII, I. & LEGROS, J.-C. 2012 *Interfacial Convection in Multilayer Systems*, 2nd edn. Springer.

POTOTSKY, A., BESTEHORN, M., MERKT, D. & THIELE, U. 2004 Alternative pathways of dewetting for a thin liquid two-layer film. *Phys. Rev.* E **70**, 025201.

POTOTSKY, A., BESTEHORN, M., MERKT, D. & THIELE, U. 2005 Morphology changes in the evolution of liquid two-layer films. *J. Chem. Phys.* **122**, 224711.

https://doi.org/10.1017/jfm.2018.304 Published online by Cambridge University Press

SMITH, K. A. 1966 On convective instability induced by surface-tension gradients. *J. Fluid Mech.* **24**, 401–414.

TAKASHIMA, M. 1981 Surface tension driven instability in a horizontal liquid layer with a deformable free surface. *J. Phys. Soc. Japan* **50**, 2745–2750.

TIWARI, N., MESTER, Z. & DAVIS, J. M. 2007 Stability and transient dynamics of the thin liquid films flowing over locally heated surfaces. *Phys. Rev.* E **76**, 056306.

https://doi.org/10.1017/jfm.2018.304 Published online by Cambridge University Press